ELSEVIER

The isotopic effects of electron transfer: An explanation for Fe isotope fractionation in nature

Abby Kavner,[1,2,*] François Bonet,[3] Anat Shahar,[1] Justin Simon[1] and Edward Young[1,2]

[1]Earth and Space Sciences Dept. UCLA, Los Angeles, CA 90095 USA
[2]Institute of Geophysics and Planetary Physics UCLA, Los Angeles, CA 90095 USA
[3]Dept. of Materials Science and Engineering UCLA, Los Angeles, CA 90095 USA

Abstract—Isotope fractionation of electroplated Fe was measured as a function of applied electrochemical potential. As plating voltage was varied from −0.9 V to 2.0 V, the isotopic signature of the electroplated iron became depleted in heavy Fe, with $\delta^{56}Fe$ values (relative to IRMM-14) ranging from −0.18(±0.02) to −2.290(±0.006) ‰, and corresponding $\delta^{57}Fe$ values of −0.247(±0.014) and −3.354(±0.019) ‰. This study demonstrates that there is a voltage-dependent isotope fractionation associated with the reduction of iron. We show that Marcus's theory for the kinetics of electron transfer can be extended to include the isotope effects of electron transfer, and that the extended theory accounts for the voltage dependence of Fe isotope fractionation. The magnitude of the electrochemically-induced fractionation is similar to that of Fe reduction by certain bacteria, suggesting that similar electrochemical processes may be responsible for biogeochemical Fe isotope effects. Charge transfer is a fundamental physicochemical process involving Fe as well as other transition metals with multiple isotopes. Partitioning of isotopes among elements with varying redox states holds promise as a tool in a wide range of the Earth and environmental sciences, biology, and industry. *Copyright © 2005 Elsevier Ltd*

1. INTRODUCTION

Recent developments in mass spectrometry techniques have created opportunities to examine the partitioning behavior of stable isotopes of transition metals (Belshaw et al., 2000; Hirata et al., 2003; Malinovsky et al., 2003; Albarède and Beard, 2004; Archer and Vance, 2004; Arnold et al., 2004), with a focus on application to iron isotopes (Beard and Johnson, 1999; Beard et al., 1999; Johnson and Beard, 1999; Polyakov and Mineev, 2000; Brantley et al., 2001; Zhang et al., 2001; Kehm et al., 2003; Anbar, 2004). Attention has focused on Fe as a biologic marker because of its ubiquity throughout the solar system, and the association of Fe oxides such as magnetite with evidence for the presence of life in some environments here on Earth (Kostka and Nealson, 1995; Cummings et al., 2000; Cox et al., 2002), and potentially, on Mars (Frankel and Buseck, 2000; Nealson and Cox, 2002). Results thus far show that most igneous rocks from the Earth and Moon show a narrow range of Fe isotopic ratios, with less than 0.5 ‰ deviations from the relative isotopic abundances of ^{56}Fe (~91.72%), ^{54}Fe (5.9%) and ^{57}Fe (2.1%) (Walker et al., 1989; Sharma et al., 2001; Beard et al., 2003a, 2003b; Wiesli et al., 2003) while variations in chemical sediments are much larger with deviations from the nominal average abundances from + 1 ‰ to −2.5 ‰ (Johnson et al., 2003; Matthews et al., 2004).

Iron oxidizing and reducing bacteria have been shown to cause isotope fractionations similar in magnitude to those observed in sedimentary environments, and it is believed that biologic activity is responsible for the most significant Fe isotope fractionation in natural settings (Mandernack et al., 1999; Brantley et al., 2001; Croal et al., 2004). For this reason

it has been suggested that Fe isotope fractionation might be an indicator of the presence of life in extreme environments on Earth and on other planets (Beard and Johnson, 1999; Beard et al., 1999; Beard et al., 2003a; Beard et al., 2003b).

Debate over the use of Fe isotopes as a biologic marker resulted from subsequent measurements of fractionations in a variety of abiotic systems including natural (Rouxel et al., 2003; Icopini et al., 2004) and laboratory environments (Zhu et al., 2000; Bullen et al., 2001; Skulan et al., 2002; Welch et al., 2003), including chromatographic separation (Anbar et al., 2000), Fe^{+2}/Fe^{+3} complex precipitation (Matthews et al., 2001), and from measurements (Polyakov, 1997; Johnson et al., 2001; Johnson et al., 2002; Roe et al., 2003) and predictions (Schauble et al., 2001; Jarzecki et al., 2004) of equilibrium fractionations between ferric-ferrous complexes. However, the fundamental physical and chemical mechanisms responsible for both natural abiotic and biotic fractionations are not yet well understood (Anbar, 2004). The accumulated evidence in both biotic and abiotic systems points to a connection between Fe oxidation-reduction processes and Fe isotope fractionation (Zhu et al., 2002). The purpose of this research program is to explore that link from a combined theoretical and experimental approach.

Electron charge transfer is the fundamental physical chemical process which occurs when an electron travels from one species to another, either via an intermediate complex, or as a single step, such as quantum mechanical tunneling (Barbara et al., 1996; Adams et al., 2003). Energy derived from charge transfer reactions is central to the existence of life (Devault, 1980; Bertrand, 1991; Bixon and Jortner, 1999; Daizadeh et al., 2002; Nealson et al., 2002). Charge transfer reactions occur at interfaces (Brown et al., 1999) and analysis of the physical chemistry at interfaces greatly informs our understanding of biochemistry (Eggleston, 1999; Eggleston et al., 2003; Neal et

* Author to whom correspondence should be addressed (akavner@ucla.edu).

al., 2003). For these reasons, an understanding of the kinetics of charge transfer processes involving Fe, and potential links between charge transfer and isotope fractionation, should provide insights into how biologic processes create isotopic signatures among the transition metals.

In this paper we extend Marcus's theory for the kinetics of electron transfer to show that there should be a kinetic isotope fractionation associated with electron transfer. We substantiate the theory by measuring a voltage dependent isotope fractionation effect in the $Fe^{+2}/Fe_{(metal)}$ system that compares favorably with the predictions.

2. A THEORY FOR THE KINTIC ISOTOPE EFFECTS OF ELECTRON TRANSFER

The isotopic effects of charge transfer can be derived with reference to the kinetic theory developed by Marcus (1964, 1965). For a review of Marcus's theory, see articles in *Chemical Reviews*, vol. 92, issue 3. Here we provide a brief review emphasizing possible isotope-dependent terms.

The rate constant k for the electron transfer reaction can be written in the usual way as

$$k = \nu \ \exp(-\Delta G^*/(k_b T)) \tag{1}$$

The pre-exponential collision frequency term ν accounts for translation

$$\nu = \left(\frac{k_b T}{2\pi m} \right)^{1/2} \tag{2}$$

where m is the appropriate mass in motion (in the present case ν refers to the collision frequency with an electrode), k_b is Boltzmann's constant and T is temperature. ΔG^* is a free energy of activation, and is analogous to the term ΔF^* in Marcus (1964, 1965). ΔG^* is composed of three distinct contributions: 1) the work required to bring reactants together; 2) a reorganization energy involving changes in bond lengths and angles as preludes to electron transfer; and 3) the difference in configurational free energy between products and reactants (free energy of reaction). For the rest of the discussion we assume that the work terms are negligible with respect to the observed isotope effects.

Following Marcus (1964, 1965), the activation energy is obtained by considering two parabolas representing the energy surfaces for the reactants and products (Fig. 1). The parabolas are one-dimensional representations along a single reaction coordinate ξ (representing changes in bond distances and reorientation of solvent molecules, for example) of what are actually multidimensional energy surfaces. The equations for the energy parabolas for reactants (r) and products (p) are

$$E_r = f\xi^2 \tag{3}$$

and

$$E_p = f(\xi - \Delta\xi)^2 + \Delta G \tag{4}$$

respectively, where E_r and E_p are the energies for the reactants and products; ΔG is the free energy difference between products and reactants; f is a force constant (N m^{-1}), and $\Delta\xi$ is a displacement along the reaction coordinate ξ between stable products and reactants (Fig. 1a). The two parabolas intersect at
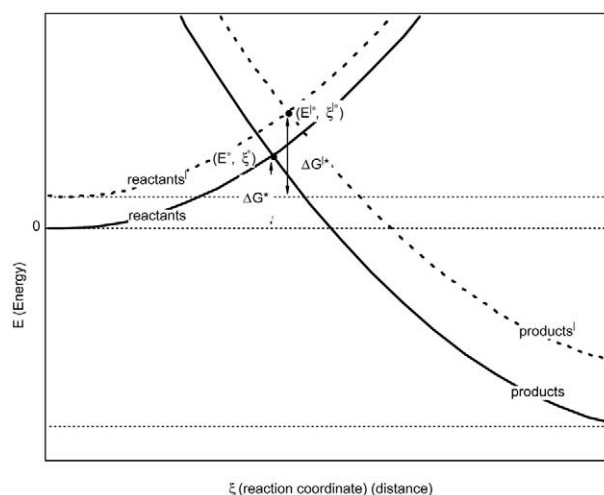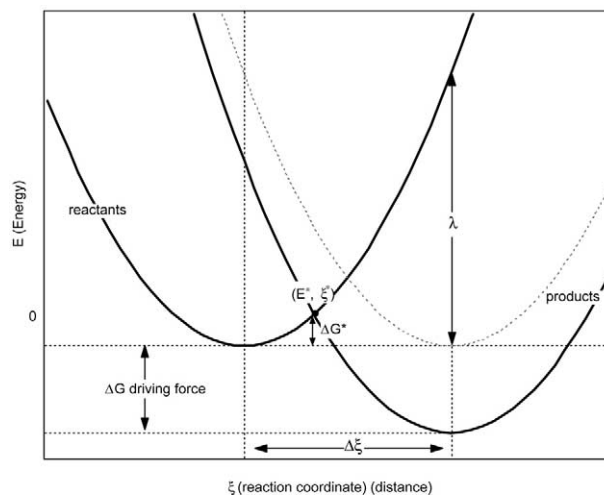

Fig. 1. a) The energy-reaction coordinate model. Reactants and products are parabolic in reaction coordinate space. Electron transfer takes place at the coordinate (E*, ξ*). The driving force for the reaction is $\Delta G = -KT \ln (Q_p/Q_r) - zeV_{appl}$. The isotope energy differences are too small to be viewed on this scale. b) A close-up of the energy-reaction coordinate model, including isotope energy differences. Energy curves for a second isotope system are depicted as dotted lines, with corresponding reaction coordinate (E'*, ξ'*).

some value of the reaction coordinate ξ* and energy E*. The difference in energy between this point of intersection and the stable energy of the reactants defines the activation free energy ΔG*. One can combine Eqn. 3 and 4 to solve the expression $E_r = E_p$ for the value of ξ* at the crossing point, yielding

$$f\xi^{*2} = f(\xi^* - \Delta\xi)^2 + \Delta G \tag{5}$$

and therefore

$$\xi^* = \frac{1}{2} \left(\Delta\xi + \frac{\Delta G}{f\Delta\xi} \right). \tag{6}$$

Substituting (6) into (3) gives the energy at ξ*

$$E^* = \frac{f\Delta\xi^2}{4} + \frac{\Delta G}{2} + \frac{\Delta G^2}{4f\Delta\xi^2} \tag{7}$$
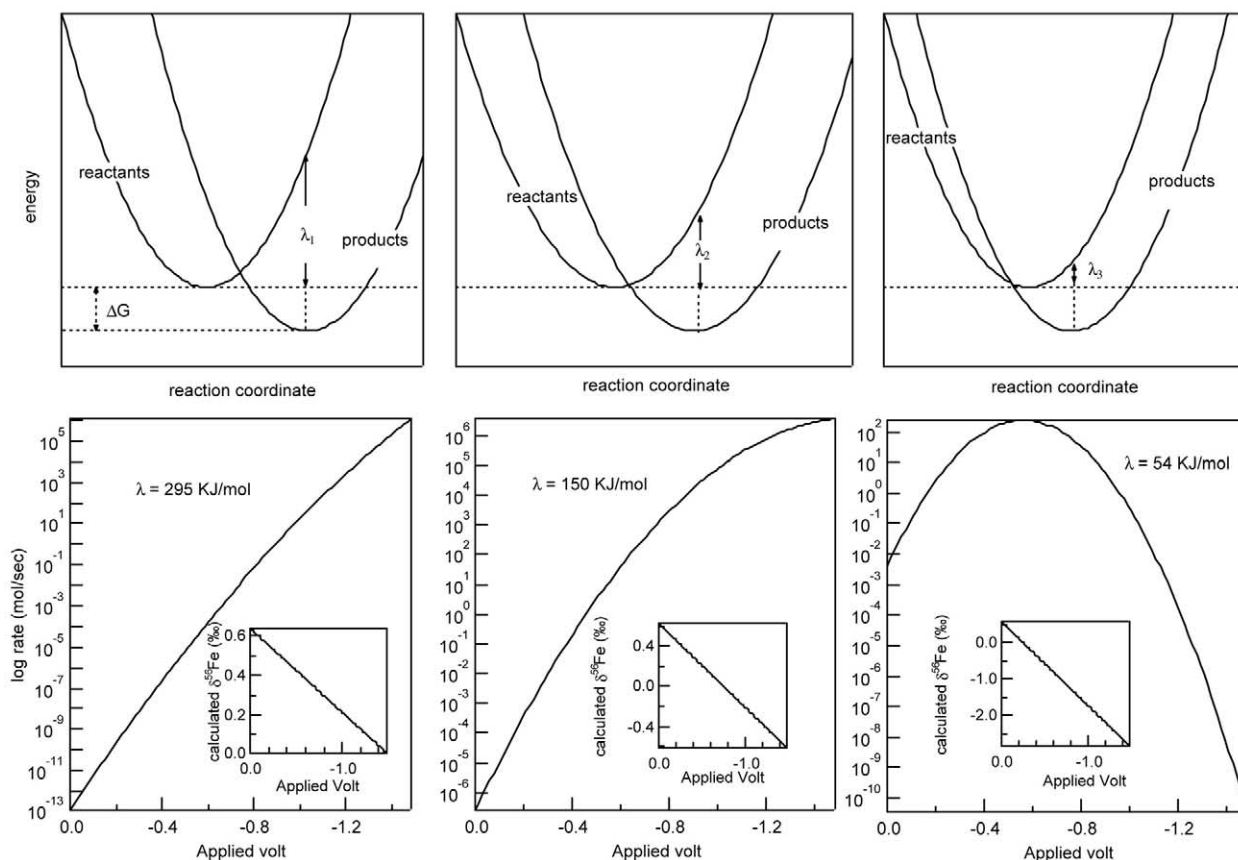
Fig. 2. Kinetic behavior of charge transfer reactions, at a range of distance coordinates. The top three figures show the reaction coordinate diagram with identical driving force, and decreasing λ proceeding from left to right. The bottom three plots depict the corresponding reaction rates as a function of driving force for each case. The inset shows the corresponding predicted voltage dependent isotope fractionation for Fe 56/54 (see text).

The value E^* is seen to be the activation free energy ΔG^* since we can arbitrarily set E_r to zero. In the context of Marcus theory, $f\Delta\xi^2$ in (7) is the "reorganization energy," λ (J), that accounts for the energy required to ready the reactants for electron transfer. Following this convention we can rewrite Eqn. 7 as

$$\Delta G^* = \frac{\lambda}{4} + \frac{\Delta G}{2} + \frac{\Delta G^2}{4\lambda}. \qquad (8)$$

According to this description of the kinetics, the reaction rate increases with increasing driving force until it attains a maximum, after which it begins to decrease with further increases in driving force. This "reverse kinetic" effect (Fig. 2) is a hallmark of Marcus theory and was confirmed experimentally by Miller et al. (1984).

To examine isotope effects, we make the simplifying assumption that λ is isotope independent and focus on terms that may show a voltage dependent isotope fractionation effect. The effect of isotope substitution on ΔG^* is through the difference in free energy between isotopologues at equilibrium (Fig. 1b). This difference in G is well known (Bigeleisen and Mayer, 1947; Bigeleisen, 1949, 1955) and is equal to $-k_b T \ln \alpha_{eq}$. The term α_{eq} is the isotope fractionation factor defined as R_p/R_a where R_p and R_a are the ratios of the rare isotopologue to the

primary isotopologue for products and reactants, respectively, at equilibrium. Said another way, α_{eq} is the ratio of reduced partition functions for the product isotopologues (Q_p'/Q_p where Q_p is the reduced partition function for the product and $'$ designates the rare isotopic species) divided by the analogous reduced partition function ratio for the reactants. In the case of the partitioning between ^{56}Fe and ^{54}Fe, for example, $\alpha_{eq} = (^{56}Fe/^{54}Fe)_p / (^{56}Fe/^{54}Fe)_r = (Q'/Q)_p/(Q'/Q)_r$.

From the known energy effects of isotope substitution we can write an equation analogous to Eqn. 8 for the activation free energy for the electron transfer reaction but for the different product and reactant isotopologues (values for the new isotope-substituted species are designated with a superscript):

$$\Delta G^{*\prime} = \frac{\lambda}{4} + \frac{(\Delta G - k_b T \ln \alpha)}{2} + \frac{(\Delta G - k_b T \ln \alpha)^2}{4\lambda}. \qquad (9)$$

The free energy change in the presence of a voltage potential will be

$$\Delta G = -k_b T \ln (Q_p/Q_r) - Vze \qquad (10)$$

where Q_p and Q_r are the partition functions for the abundant isotopologue of the product and reactant; V is the applied voltage (with the convention that negative V is cathodic

A. Kavner et. al.

potential); z is the number of electrons transferred; and e is the charge of an electron. Eqn. 10 is equivalent to $\Delta G = -(V - V_0)ze$, where V_0 is the equilibrium potential.

The kinetic isotope fractionation factor, α_{kinetic}, describes the isotope partitioning arising from kinetics and is related to the ratio of the rate constants for the two different isotopologues in the electron transfer reaction such that

$$\ln \alpha_{\text{kinetic}} = \ln \left(\frac{k'}{k} \right) = \ln \left(\frac{v'}{v} \right) + ((\Delta G^* - \Delta G^{*\prime})/(k_b T)). \quad (11)$$

The kinetic isotope fractionation factor can be cast into per mil deviations from the original reactant isotopic ratio using the "linearized" delta notation where $\delta_{p-r} = 10^3 \ln \alpha_{\text{kinetic}}$. Substitution of (2), (8), (9) and (10) into (11) yields the equation for per mil fractionation as result of the kinetics of electron transfer:

$$\frac{\delta_{p-r}}{10^3} = \frac{1}{2} \ln \left(\frac{m}{m'} \right) - \frac{Vze}{2\lambda} \ln \alpha_{\text{eq}} + \frac{1}{2} \ln \alpha_{\text{eq}} - \frac{k_b T}{4\lambda} (\ln \alpha_{\text{eq}})^2$$
$$- \frac{k_b T}{2\lambda} \ln \left(\frac{Q_p}{Q_r} \right) \ln \alpha_{\text{eq}}. \quad (12)$$

From Eqn. 12 comes the prediction that there should be a kinetic isotope fractionation associated with an electron transfer reaction, and that this fractionation will depend on the applied voltage that drives the reaction (Fig. 2).

The extension of the Marcus theory for the kinetics of electron transfer predicts a linear relationship between δ_{p-r} and voltage V where the slope is

$$\frac{\partial \delta_{p-r}}{\partial V} = -10^3 \frac{ze}{2\lambda} \ln \alpha_{\text{eq}} \quad (13)$$

and the intercept B is

$$B = 10^3 \left[\frac{1}{2} \ln \left(\frac{m}{m'} \right) + \frac{1}{2} \ln \alpha_{\text{eq}} - \frac{k_b T}{4\lambda} (\ln \alpha_{\text{eq}})^2 \right.$$
$$\left. - \frac{k_b T}{2\lambda} \ln \left(\frac{Q_p}{Q_r} \right) \ln \alpha_{\text{eq}} \right]. \quad (14)$$

The magnitude of the kinetic isotope effect is predicted to be a balance between the fractionation imparted by translation, the maximum value of which is represented by the first term in Eqn. 14, and the effect of the reduced partition function ratios represented by the $\ln \alpha_{\text{eq}}$ terms. In practice, the translation term will be considerably smaller than the first term in Eqn. 14 while the last term in Eqn. 14 is generally negligible. The sign of the slope of fractionation vs. voltage depends on the sign of $\ln \alpha_{\text{eq}}$. When the products are enriched in the rare isotope relative to the reactants at equilibrium, α_{eq} is greater than 1 and $\ln \alpha_{\text{eq}}$ is positive, resulting in a positive slope. When the products are depleted in the rare isotope relative to the reactants at equilibrium, $\ln \alpha_{\text{eq}}$ is negative and the slope of voltage-dependent fractionation will be negative.

The prediction of a voltage-dependent isotope effect during electron transfer does not result from applying simple equations relating reaction rate to applied voltage (e.g., the overpotential-
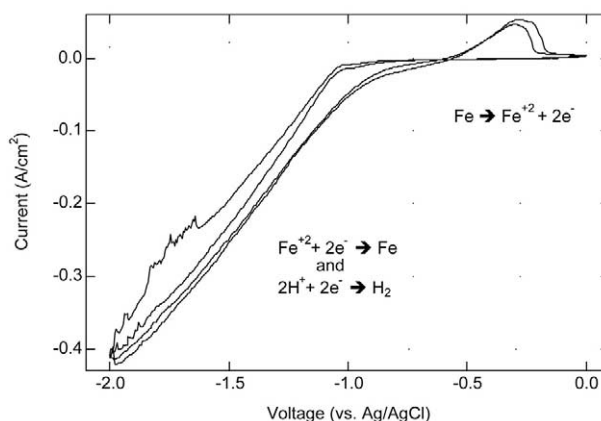

Fig. 3. Cyclic Voltammetry plot of $FeCl_2$ + HCl liquid on a glassy carbon electrode using a scan rate of 10 mV/s. This plot shows how current varies as a function of applied voltage (with respect to a standard electrode) for the starting plating solution, during two cycles. At the larger negative voltages, the current increase (absolute value) is due to both plating of iron and reduction of $2H^+$ to H_2 gas. The hump of positive current at voltages between −0.5 and 0 V is due to oxidation of the iron plated in the previous reduction cycle.

activated Butler-Volmer equation (Bockris and Reddy, 1970; Bard and Faulkner, 1980). It is a natural result of Marcus's theory, however, making it possible to test the isotope-specific extension to Marcus theory by examining the effects of voltage on isotope fractionation during redox reactions.

3. FE ELECTROPLATING EXPERIMENTS

The prediction that isotope fractionation associated with electron transfer should depend on applied voltage was verified in this study experimentally. We report here a kinetic voltage-dependent isotope effect for Fe that is consistent with the predictions of Eqn. 12.

3.1. Electrochemistry

Iron electroplating experiments were performed under potentiostat conditions with an EG&G Potentiostat model 273 using a three-electrode electrochemical cell, equipped with a Ag/AgCl reference electrode and glassy carbon counter electrode. Potentials are reported with respect to the Ag/AgCl reference electrode unless otherwise noted. The electroplating bath consisted of 20 mL aliquots from an initial 1L stock of 2M $FeCl_2$ acidified with 1 M HCl. Before each experiment, the solution was de-oxygenated with bubbling N_2 for 20 min. Cyclic voltammetry (CV) tests of the plating bath (Fig. 3) show voltage-activated kinetics, with cathodic reactions below −0.9 V and iron oxidation above −0.5 V. In all cases, the cathodic reaction was a combination of iron deposition and hydrogen evolution, consistent with the observed active bubbling at the working electrode.

Each electroplating experiment was performed with a fresh ~1 cm^2 glassy carbon electrode. Two sets of plating experiments were performed. The first set consisted of two plating experiments, at −0.9V and −1.25 V. The second set consisted of deposition potentials of −0.7, −0.9, −1.1, −1.25, −1.5, and −2.0 V. Plating times were controlled so that the same amount

Table 1. Data from each of the plating experiments.

Plating Potential[a]	δ^{56}Fe (‰)	δ^{57}Fe (‰)	Amount deposited[e] (mg)	Deposition efficiency (%)	Average current (A/cm^2)	Total time (sec)
Starting material 1	−0.184 (0.014)[b]	−0.252 (0.031)				
−1.25 (1)	−1.543 (0.010)	−2.320 (0.011)	1.5	5.5	0.02	4508
−0.9 (1)	−0.252 (0.008)	−0.349 (0.021)	1.5	6.3	0.008	10600
Starting material 2	−0.171 (0.013)	−0.249 (0.025)				
−2.0	−2.290 (0.006)	−3.354 (0.019)	0.2	0.9	0.15	540
−1.5	−1.753 (0.007)	−2.591 (0.027)	0.3	0.9	0.10	970
−0.9	−0.106 (0.010)	−0.145 (0.011)	0.1	0.9	0.002	26330
−1.1	−0.655 (0.012)	−0.951 (0.023)	0.3	0.9	0.03	3210
−1.25	−1.686 (0.010)	−2.498 (0.020)	0.2	0.7	0.052	1550
−0.7[c]	N/A	N/A	N/A	N/A	0.00003	35990
−1.25[d]	−0.546 (0.013)	−0.802 (0.029)	0.09	0.4	0.05	1400
	−0.552 (0.014)	−0.784 (0.021)				

[a] Potentials are given versus the Ag/AgCl reference electrode.
[b] Error bars for delta values are one-sigma error bars.
[c] Experiment terminated after ten hours—too low a voltage to electroplate.
[d] Experiment agitated by N$_2$ bubbling during plating. H$_2$ evolution efficiency greater.
[e] Efficiency is a lower bound, due to possible flaking off of electroplated iron during plating.

of total charge density ($\sim$75–100 C/cm^2) was exchanged in all cases. Electroplating times in the second experiment varied from 9 min (in −2.0 V experiment) to over 7 hours (−0.9 V). The amount of electrodeposited iron was consistent within each set of experiments, with the first set ($\sim$1–2 mg) significantly more efficient than the second set ($\sim$0.1–0.3 mg). The amount plated is $\sim$0.03% of the initial concentration of Fe within the plating bath for the first set of experiments, and 0.002–0.005% for the second set. The small amount plated, compared with the 80 Coulombs of charge passed for each experiment indicates the low efficiency of the iron plating process, compared with hydrogen evolution. The plating efficiency does not vary as a function of plating potential. An additional experiment was performed at −1.25 V with continuous N$_2$ sparging.

3.2. Wet Chemistry

Each electrode was collected and gently washed with distilled water to remove the plating bath. The electrodes were then placed in clean Teflon beakers. Electroplated iron was removed from the electrodes with hot concentrated HNO$_3$ acid for about six hours followed by hot concentrated HCl acid for about ten hours. The solutions were dried down after acid baths, and were finally re-dissolved in 0.3 N nitric acid for analysis. The samples were diluted to an iron concentration of $\sim$5 ppm Fe in the first set of experiments, and $\sim$3.8 ppm in the second set of experiments. In addition, to provide a control the starting material FeCl$_2$ was dissolved in hot concentrated HNO$_3$ acid and then diluted to 0.3 N for analysis.

3.3. Mass Spectrometry

The Fe isotopic compositions of plating experiments were determined by sample-standard comparisons using a multi-collector inductively-coupled plasma mass spectrometer (MC-ICPMS) (ThermoFinnigan Neptune) at UCLA. Solutions were found to be effectively pure; trace amounts of ^{52}Cr, the most abundant Cr isotope ($>$83%), were negligible; there was no

measurable mass interference at mass 54 (e.g., background ^{52}Cr signals of 5 mV corresponding to a 0.1 mV ^{54}Cr background signal compared with sample ^{54}Fe signals of several volts). Peak heights for sample and standard were matched to minimize background effects. Mass interferences from ArO$^+$, ArOH$^+$ and ArN$^+$ were resolved from the ^{56}Fe, ^{57}Fe and ^{54}Fe peaks by operating at a mass resolving power of $\sim$12,000 (corresponding to a flat-top peak mass resolution of 4000). Potential instrumental mass bias due to interelement matrix effects was not an issue since measurements were made on dilute and pure Fe solutions. Each solution was analyzed 5 to 6 times. Mean values for δ^{56}Fe and δ^{57}Fe and their corresponding standard deviations for the means (standard errors) are reported in Table 1. We report ^{56}Fe/^{54}Fe and ^{57}Fe/^{54}Fe of reactant and product Fe as the per mil deviations from the IRMM-14 Fe isotope standard (Taylor, 1999) using the δ notation where:

$$\delta^{56}Fe = ((^{56}Fe/^{54}Fe)_{sample}/(^{56}Fe/^{54}Fe)_{IRMM-14} - 1) * 1000$$

$$\delta^{57}Fe = ((^{57}Fe/^{54}Fe)_{sample}/(^{57}Fe/^{54}Fe)_{IRMM-14} - 1) * 1000$$

$$(15)$$

4. RESULTS

4.1. Voltage-Dependent Fractionation

Results (Table 1, Fig. 4) show that isotopically light iron is preferentially electroplated, and the amount of light isotope enrichment depends on applied voltage. δ^{56}Fe values range from −0.18($\pm$0.02) ‰ at a potential of −0.9 V to −2.290($\pm$0.006) ‰ at a potential of −2.0V. Corresponding values for δ^{57}Fe are −0.247($\pm$0.014)‰ and −3.354(0.019) ‰. The δ^{56}Fe and δ^{57}Fe values for the Fe^{+2} in the starting solution are −0.176(0.014) ‰ and −0.251(0.030) ‰, respectively. Results from two separate sets of experiments are in good agreement (as shown by the values at −0.9 V and −1.25 V) despite over an order of magnitude difference between them in plating efficiency, and slight differences in experimental pro-
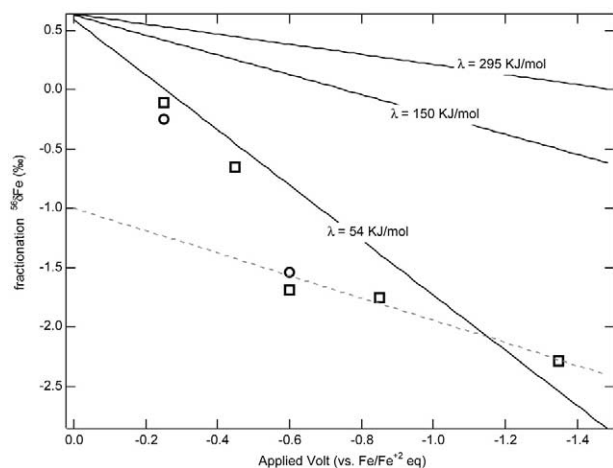
Fig. 4. $\delta^{56}Fe$ values as a function of applied voltage (referenced to the equilibrium potential for the Fe^{+2}/Fe reaction) for the recovered plated iron from the potentiostatic (constant voltage) electroplating experiments. The two separate sets of experiments are depicted as circles and squares. Calculated fractionations for three different values of λ are also displayed on this plot. The dashed gray line is the best-fit regression through the portion of the data lying on the linear part of the CV curve.
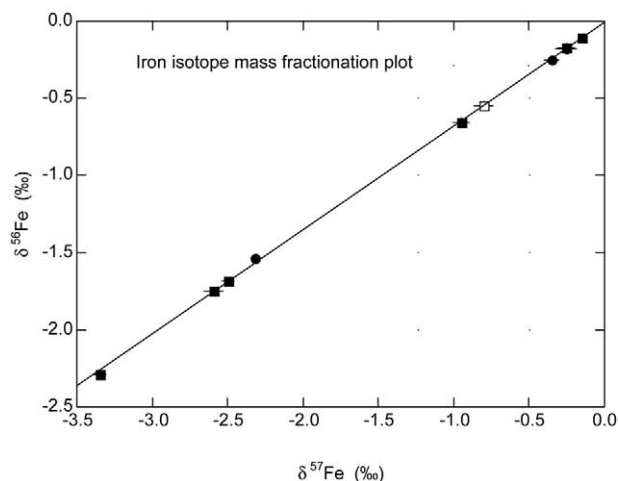

Fig. 5. Three isotope plot for all of the iron isotope fractionation data from the nine electroplating experiments. Circles and squares correspond to the two experimental runs. The measurement performed during N_2 bubbling is depicted as an open symbol. This plot shows one-sigma error bars on the measurements.

cedures, including different starting solutions (mixed from different aliquots of the same starting materials), some differences in wet chemistry technique, and a month-long timescale between experimental sets. With these results, we have demonstrated a quantitative link between the driving force for a charge transfer reaction, and a resulting geochemical signature.

An exception to this trend was observed in the single electroplating experiment performed with concurrent N_2 bubbling. Although the original goal of this experiment was to provide a simple constraint on the effects of mixing, in actuality, many different experimental variables were affected, including different hydrodynamics, aqueous chemistry, and relative hydrogen reduction/iron reduction rates. In addition, the CV plot for this experiment was noisy at the 20% level, unlike the experiments performed without gas bubbling. Therefore, we do not consider this single experiment to provide useful additional information, and plan instead to explore mass transport effects systematically using a rotating disk electrode system.

This voltage-dependent fractionation effect seen here has never before been observed in Fe or any other transition metal system. However, it is not entirely unprecedented. Similar observations of electrochemically-driven isotopic fractionation in the hydrogen-deuterium system have been reported (Topley and Eyring, 1934; Urey, 1947). In these experiments, the lighter hydrogen isotope had a faster electrochemical reaction rate, leaving behind a liquid enriched in deuterium.

4.2. Three-Isotope Plot

The relationship between $^{56}Fe/^{54}Fe$ (^{56}R) and $^{57}Fe/^{54}Fe$ (^{57}R) of the experimental products constitutes an exponential mass fractionation law among the three isotopes which is characterized by an exponent β, the values of which are diagnostic of the type of process, (e.g., kinetic or equilibrium) that caused the fractionation (Young et al., 2002). This value is

similar to, but not exactly, the slope of the three isotope plot (Fig. 5). The β for processes governed by reduced partition function ratios has a high temperature limit of $(1/m_{54}-1/m_{56})/(1/m_{54}-1/m_{57})$ where m_i is the atomic mass of the indicated Fe isotope. Slopes with this functional form are referred to as "equilibrium" slopes in three isotope space since they arise solely from the partition function ratios responsible for equilibrium isotope partitioning. For kinetic processes involving collective masses in motion the values for β are $\ln (M_{54}/M_{56})/\ln (M_{54}/M_{57})$ where M_i are the masses of species involved in the rate-limiting process. Slopes with this functional form arise from momentum effects independent of the reduced partition function ratio. We emphasize that the kinetic isotope effect incurred during the electroplating process does not necessitate a purely kinetic slope. For example, if isotope fractionation were to arise only from the voltage-dependent kinetic effect (e.g., Eqn. 13 or all but the 1st terms in Eqn. 12), the three isotopes would define a so-called "equilibrium" slope in three isotope space because the dominant term is a reduced partition function ratio.

The β values reported here were obtained by regressing the experimental data cast in terms of $\ln (^{56}R/^{56}R_{IRMM-14}) * 1000$ and $\ln (^{57}R/^{57}R_{IRMM-14}) * 1000$ (e.g., Young et al., 2002). Each sample was weighted by its associated standard error and the correlation coefficient between the individual replicate $\delta^{56}Fe$ and $\delta^{57}Fe$ measurements. The best-fit β value for the electroplating experiments is $0.6723(\pm 0.0032)(95\%)$. This value is statistically indistinguishable from the predicted kinetic β of 0.6720 where the masses in motion are Fe atoms (or ions) and is significantly different from the predicted high-temperature limit of reduced partition function effects. This result suggest that there is some component of molecular translation involved in the kinetics, suggesting that the first term in Eqn. 12 has some influence. The caveat is that we do not know the precise β value for the low-temperature reduced partition function ratio (often lower temperatures tend to lower the β value for the partition function ratios), making it difficult to extract quanti-

tatively the contribution of the first term in Eqn. 12 to the overall fractionation effect.

5. DISCUSSION

5.1. Comparing Experimental Results to Predictions

Electroplating consists of a large number of single step processes required to bring the solvated (or other aqueo-complexed Fe^{+2}) to the electrode surface, to generate the activated complex, to perform two electron transfers, and to nucleate and grow the metal on the electrode. (Koryta, 1959; Bockris and Reddy, 1970) Bard and Faulkner, 1980). The theory described in section 2 likely does not capture the full complexity of the reaction; however, it can provide a first-order prediction for the slope and intercept for the voltage-dependent isotope fractionation in the Fe electroplating reaction.

Equation 13 shows that the voltage-dependent contribution to the electrochemical isotope fractionation is a function of two parameters: equilibrium fractionation ($1000 \ln \alpha_{eq}$) and reorganization energies (λ) for the rate limiting step. For typical ionic stretching force constants of 500 to 900 Nm^{-1} and interatomic distances of 2×10^{-11} m, the reorganization energies are on the order of 60 to 100 KJ/mol. In aqueous solutions with $[Cl^-]$ greater than 4M, (the solution chemistry employed in these experiments uses $[Cl^-] = 5M$) Fe^{+2} likely exists as Cl^- complexed ferrous ions (e.g., Snoeyink and Jenkins, 1980). Calculations exist for equilibrium fractionation in many Fe-complexes and Fe metal (Schauble et al., 2001) using vibration energies from spectroscopy measurements. The per mil reduced partition function ratios $1000 \ln (Q^{56}/Q^{54})$ relative to dissociated atoms are 4.0 (±0.2) for $(Fe^{II}Cl_4)^{-2}$ and 5.3(±1.0) for Fe_{metal} at 25°C (i.e., the equilibrium partitioning favors ^{56}Fe in the metal). Since $1000 \ln \alpha_{eq}$ for two substances a and b is $1000 \ln (Q^{56}/Q^{54})_a - 1000 \ln (Q^{56}/Q^{54})_b$, these values yield a metal/chlorocomplex $1000 \ln \alpha_{eq}$ of 1.3. Using these values, the predicted slopes in δ^{56} vs. V space (Eqn. 12) range from 1.2 to 2.1. The data on the linear portion of the CV curve (absolute values of applied voltages greater than 1.0 V) yield a best-fit slope of 0.89 (±0.33) (95%). The agreement between the predicted slope from Marcus' theory for electron transfer and the experiments suggests that the electron transfer process is controlling the isotope kinetics.

The intercept predicted on the basis of the dominant term in Eqn. 12 is 10^3 (1/2) $\ln \alpha_{eq}$, or + 0.65 ‰. The data comprising the linear portion of the CV curve yield an intercept of -0.5 ‰. The difference can be attributed to a contribution from the preexponential component in the rate equation (i.e., first term in Eqn. 12). The maximum that translation of $FeCl_2$ isotopologues can contribute to the intercept is -8 ‰, suggesting that the contribution need not be great to significantly affect the intercept.

One major uncertainty in our data is the relative contribution to the overall plating rate by the Fe electroplating reaction compared with hydrogen evolution. Hydrogen evolution is dominating the overall rate as shown on the CV plot; in these experiments Fe plating is in strong competition. Therefore, it is unknown whether plating is occurring in the "forward" or "reverse" kinetics regimes in the context of Marcus theory. The observed fractionations would be smaller (but still comparable

to our observations) in the forward regime; in the reverse regimes, larger fractionation effects might be observed. This prediction suggests that there are classes of reactions in which very large isotope effects are expected. We look forward to testing these ideas with further experiments.

The major alternative hypothesis for the observed fractionation, mass transport effects, is likely ruled out. These electroplating experiments are not performed in a diffusion-limited regime. We know this from examining the CV plot (Fig. 3) which shows voltage activated cathodic current throughout the range of the electroplating experiments. In addition, there is active H_2 bubbling at the electrodes throughout each experiment, which provides active mixing of solution, and would destroy any significant stagnant layer. Finally, and most importantly, neither time independent nor time dependent diffusion models can generate a voltage-dependent fractionation. Therefore, we conclude that although diffusion may play some role in the observed fractionation, it is not responsible for the overall fractionation and it certainly cannot explain the observed voltage dependence.

5.2. Applicability to Natural Systems

The results shown here strongly suggest that stable isotopes systems such as Fe can be used as a quantitative marker for the driving force during electrochemical processes as described by Eqn. 12. Although in biologic systems, and in most geological systems studied, the relevant Fe species are Fe^{+2} and Fe^{+3} while our experiments were on the reduction of Fe^{+2} to Fe_{metal}, the relationship between electron transfer and isotope fractionation as described here is fundamental to any change in redox state. Interestingly, both the plating potentials applied in this experiment (~100's mV) and the resulting magnitude of Fe isotope fractionation ($\delta^{56}Fe$ of -1 to -2‰) are comparable to their counterparts in biologic systems. Similar fractionations are observed in Fe-reducing bacteria (Anbar, 2004) and biochemical studies of cell behavior indicate that the cell membrane establishes a potential gradient that is on the order of 100's of mV (e.g., Walsh, 1978; Felle et al., 1980; Capaldi, 1990; Nealson and Conrad, 1999). This similarity between the electrochemical experiment and the biologic systems suggests that the isotope-specificity of electron transfer described here may capture the fundamental mechanism of Fe isotope fractionation in at least some biochemical reactions.

Associate editor: J. Horita

REFERENCES

Adams D. M., Brus L., Chidsey C. E. D., Creager S., Creutz C., Kagan C. R., Kamat P. V., Lieberman M., Lindsay S., Marcus R. A., Metzger R. M., Michel-Beyerle M. E., Miller J. R., Newton M. D., Rolison D. R., Sankey O., Schanze K. S., Yardley J. and Zhu X. Y. (2003) Charge transfer on the nanoscale: Current status. *J. Phys. Chem. B* **107,** 6668–6697.

Albarède F., and Beard B. (2004) Analytical methods for non-traditional isotopes. In *Rev. in Mineralogy and Geochemistry, Vol. 55:*

Geochemistry of Non-Traditional Stable Isotopes (eds. C. M. Johnson, B. L. Beard and F. Albarede), pp. 113–152. Mineralogical Society of America, Washington DC.

Anbar A. D. (2004) Iron stable isotopes: beyond biosignatures. *Earth Planet. Sci. Lett.* **217,** 223–236.

Anbar A. D., Roe J. E., Barling J., and Nealson K. H. (2000) Nonbiological fractionation of iron isotopes. *Science* **288,** 126–128.

Archer C., and Vance D. (2004) Mass discrimination correction in multiple-collector plasma source mass spectrometry: an example using Cu and Zn isotopes. *J. Anal. At. Spectrom.* **19,** 656–665.

Arnold G. L., Weyer S, and Anbar A. D. (2004) Fe isotope variations in natural materials measured using high mass resolution multiple collector ICPMS. *Anal. Chem.* **76,** 322–327.

Barbara P. F., Meyer T. J, and Ratner M. A. (1996) Contemporary issues in electron transfer research. *J. Phys. Chem.* **100,** 13148–13168.

Bard A. J., and Faulkner L. R. (1980) Electrochemical Methods, Fundamentals and Applications. Wiley, 718pp.

Beard B. L., and Johnson C. M. (1999) High precision iron isotope measurements of terrestrial and lunar materials. *Geochim. Cosmochim. Acta* **63,** 1653–1660.

Beard B. L., Johnson C. M., Cox L., Sun H., Nealson K. H., and Aguilar C. (1999) Iron isotope biosignatures. *Science* **285,** 1889–1892.

Beard B. L., Johnson C. M., Skulan J. L., Nealson K. H., Cox L., and Sun H. (2003a) Application of Fe isotopes to tracing the geochemical and biological cycling of Fe. *Chem. Geol.* **195,** 87–117.

Beard B. L., Johnson C. M., Von Damm K. L., and Poulson R. L. (2003b) Iron isotope constraints on Fe cycling and mass balance in oxygenated Earth oceans. *Geology* **31,** 629–632.

Belshaw N. S., Zhu X. K., Guo Y., and O'Nions R. K. (2000) High precision measurement of iron isotopes by plasma source mass spectrometry. *Int. J. Mass Spectrom.* **197,** 191–195.

Bertrand P. (1991) Application of Electron-Transfer Theories to Biological-Systems. *Struct. Bond.* **75,** 3–47.

Bigeleisen J. (1949) The relative reaction velocities of isotopic molecules. *J. Chem. Phys.* **17,** 675–678.

Bigeleisen J. (1955) Staticstical mechanics of isotopic systems with small quantum corrections. I. General considerations and the rule of the geometric mean. *J. Chem. Phys.* **23,** 2264–2267.

Bigeleisen J., and Mayer M. G. (1947) Calculation of Equilibrium constants for isotopic exchange reactions. *J. Chem. Phys.* **15,** 261–267.

Bixon M., and Jortner J. (1999) Electron transfer—From isolated molecules to biomolecules. *Adv. Chem. Phys.* **106,** 35–202.

Bockris J. O. M., and Reddy A. K. N. (1970) Modern Electrochemistry. New York, 1432 pp. Plenum Press.

Brantley S. L., Liermann L., and Bullen T. D. (2001) Fractionation of Fe isotopes by soil microbes and organic acids. *Geol.* **29,** 535–538.

Brown G. E., Henrich V. E., Casey W. H., Clark D. L., Eggleston C., Felmy A., Goodman D. W., Gratzel M., Maciel G., McCarthy M. I., Nealson K. H., Sverjensky D. A., Toney M. F., and Zachara J. M. (1999) Metal oxide surfaces and their interactions with aqueous solutions and microbial organisms. *Chem. Rev.* **99,** 77–174.

Bullen T. D., White A. F., Childs C. W., Vivit D. V., and Schulz M. S. (2001) Demonstration of significant abiotic iron isotope fractionation in nature. *Geol.* **29,** 699–702.

Capaldi R. A. (1990) Structure and function of cytochrome c oxidase. *Ann. Rev. Biochem.* **59,** 569–596.

Cox B. L., Popa R., Bazylinski D. A., Lanoil B., Douglas S., Belz A., Engler D. L., and Nealson K. H. (2002) Organization and elemental analysis of P-, S- and Fe-rich inclusions in a population of freshwater magnetococci. *Geomicrobiol. J.* **19,** 387–406.

Croal L. R., Johnson C. M., Beard B. L., and Newman D. K. (2004) Iron isotope fractionation by Fe(II)-oxidizing photoautotrophic bacteria. *Geochim. Cosmochim. Acta* **68,** 1227–1242.

Cummings D. E., March A. W., Bostick B., Spring S., Caccavo F., Fendorf S., and Rosenzweig R. F. (2000) Evidence for microbial Fe(III) reduction in anoxic, mining-impacted lake sediments (Lake Coeur d'Alene, Idaho). *Appl. Environ. Microbiol.* **66,** 154–162.

Daizadeh I., Medvedev D. M., and Stuchebrukhov A. A. (2002) Electron transfer in ferredoxin: Are tunneling pathways evolutionarily conserved? *Molec. Biol. Evol.* **19,** 406–415.

Devault D. (1980) Quantum-Mechanical Tunnelling in Biological-Systems. *Quart. Rev. Biophys.* **13,** 387–564.

Eggleston C. M. (1999) The surface structure of α-Fe$_2$O$_3$ (001) by scanning tunneling microscopy: Implications for interfacial electron transfer reactions. *Am. Miner.* **84,** 1061–1070.

Eggleston C. M., Stack A. G., Rosso K. M., Higgins S. R., Bice A. M., Boese S. W., Pribyl R. D., and Nichols J. J. (2003) The structure of hematite (α-Fe$_2$O$_3$) (001) surfaces in aqueous media: Scanning tunneling microscopy and resonant tunneling calculations of coexisting O and Fe terminations. *Geochim. Cosmochim. Acta* **67,** 985–1000.

Felle H., Porter J. S., Slayman C., and Kaback H. (1980) Quantitative measurements of membrane potential in Escherichia coli. *Biochem.* **19,** 3585–3590.

Frankel R. B., and Buseck P. R. (2000) Magnetite biomineralization and ancient life on Mars. *Curr. Opin. Chem. Biol.* **4,** 171–176.

Hirata T., Hayano Y., and Ohno T. (2003) Improvements in precision of isotopic ratio measurements using laser ablation-multiple collector-ICP-mass spectrometry: reduction of changes in measured isotopic ratios. *J. Anal. At. Spectrom.* **18,** 1283–1288.

Icopini G. A., Anbar A. D., Ruebush S. S., Tien M., and Brantley S. L. (2004) Iron isotope fractionation during microbial reduction of iron: The importance of adsorption. *Geol.* **32,** 205–208.

Jarzecki A., Anbar A. D., and Spiro T. (2004) DFT analysis of Fe(H$_2$O)$_6{}^{2+}$ and Fe(H$_2$O)$_6{}^{2+}$ structure and vibrations; implications for isotope fractionation. *J. Phys. Chem. A* **108,** 2726–2732.

Johnson C. M., and Beard B. L. (1999) Correction of instrumentally produced mass fractionation during isotopic analysis of Fe by thermal ionization mass spectrometry. *Int. J. Mass Spectrom.* **193,** 87–99.

Johnson C. M., Beard B. L., Beukes N. J., Klein C., and O'Leary J. M. (2003) Ancient geochemical cycling in the Earth as inferred from Fe isotope studies of banded iron formations from the Transvaal Craton. *Contrib. Mineral. Petrol.* **144,** 523–547.

Johnson C. M., Skulan J. L., Beard B., Sun H., Nealson K. H., and Braterman P. S. (2001) Isotopic fractionation between Fe(III) and Fe(II) in aqueous solutions. *Earth Planet. Sci. Lett.* **195,** 141–153.

Johnson C. M., Skulan J. L., Beard B. L., Sun H., Nealson K. H., and Braterman P. S. (2002) Isotopic fractionation between Fe(III) and Fe(II) in aqueous solutions. *Earth Planet. Sci. Lett.* **195,** 141–153.

Kehm K., Hauri E. H., Alexander C. M. O., and Carlson R. W. (2003) High precision iron isotope measurements of meteoritic material by cold plasma ICP-MS. *Geochim. Cosmochim. Acta* **67,** 2879–2891.

Koryta J. (1959) Polarographic methods of investigation of the kinetics of metal deposition from complex compounds. *Electrochim. Acta* **1,** 26–31.

Kostka J. E., and Nealson K. H. (1995) Dissolution and Reduction of Magnetite by Bacteria. *Env. Sci. Technol.* **29,** 2535–2540.

Malinovsky D., Stenberg A., Rodushkin I., Andren H., Ingri J., Ohlander B., and Baxter D. C. (2003) Performance of high resolution MC-ICP-MS for Fe isotope ratio measurements in sedimentary geological materials. *J. Anal. At. Spectrom.* **18,** 687–695.

Mandernack K. W., Bazylinski D. A., Shanks W. C., and Bullen T. D. (1999) Oxygen and iron isotope studies of magnetite produced by magnetotactic bacteria. *Science* **285,** 1892–1896.

Marcus R. (1964) Chemical and electrochemical electron-transfer theory. *Ann. Rev. Phys. Chem.* **15,** 155–196.

Marcus R. (1965) On the theory of electron-transfer reactions. VI. Unified treatment for homogeneous and electrode reactions. *J. Chem. Phys.* **43,** 679–701.

Matthews A., Morgans-Bell H. S., Emmanuel S., Jenkyns H. C., Erel Y., and Halicz L. (2004) Controls on iron-isotope fractionation in organic-rich sediments (Kimmeridge Clay, Upper Jurassic, southern England). *Geochim. Cosmochim. Acta* **68,** 3107–3123.

Matthews A., Zhu X. K., and O'Nions K. (2001) Kinetic iron stable isotope fractionation between iron (-II) and (-III) complexes in solution. *Earth Planet. Sci. Lett.* **192,** 81–92.

Miller J. R., Calcaterra L. T., and Closs G. L. (1984) Intramolecular long-distance electron transfer in radical anions. The effects of free energy and solvent on the reaction rates. *J. Am. Chem. Soc.* **106,** 3047–3049.

Neal A. L., Rosso K. M., Geesey G. G., Gorby Y. A., and Little B. J. (2003) Surface structure effects on direct reduction of iron oxides

by Shewanella oneidensis. *Geochim. Cosmochim. Acta* **67,** 4489–4503.

Nealson K. H., and Conrad P. G. (1999) Life: past, present and future. *Philos. Trans. R. Soc. Lond. Ser. B-Biol. Sci.* **354,** 1923–1939.

Nealson K. H., Belz A., and McKee B. (2002) Breathing metals as a way of life: geobiology in action. *Antonie Van Leeuwenhoek Int. J. Gen. Molec. Microbiol.* **81,** 215–222.

Nealson K. H., and Cox B. L. (2002) Microbial metal-ion reduction and Mars: extraterrestrial expectations? *Curr. Opin. Microbiol.* **5,** 296–300.

Polyakov V. B. (1997) Equilibrium fractionation of the iron isotopes: Estimation from Mossbauer spectroscopy data. *Geochim. Cosmochim. Acta* **61,** 4213–4217.

Polyakov V. B., and Mineev S. D. (2000) The use of Mossbauer spectroscopy in stable isotope geochemistry. *Geochim. Cosmochim. Acta* **64,** 849–865.

Roe J. E., Anbar A. D., and Barling J. (2003) Nonbiological fractionation of Fe isotopes: evidence of an equilibrium isotope effect. *Chem. Geol.* **195,** 69–85.

Rouxel O., Dobbek N., Ludden J., and Fouquet Y. (2003) Iron isotope fractionation during oceanic crust alteration. *Chem. Geol.* **202,** 155–182.

Schauble E. A., Rossman G. R., and Taylor H. P. (2001) Theoretical estimates of equilibrium Fe-isotope fractionations from vibrational spectroscopy. *Geochim. Cosmochim. Acta* **65,** 2487–2497.

Sharma M., Polizzotto M., and Anbar A. D. (2001) Iron isotopes in hot springs along the Juan de Fuca Ridge. *Earth Planet. Sci. Lett.* **194,** 39–51.

Skulan J. L., Beard B. L., and Johnson C. M. (2002) Kinetic and equilibrium Fe isotope fractionation between aqueous Fe(III) and hematite. *Geochim. Cosmochim. Acta* **66,** 2995–3015.

Snoeyink V. L., and Jenkins D. (1980) Water Chemistry. J. Wiley & Sons, New York.

Taylor P. (1999) Certificate Isotopic Reference Material IRMM-014. Institute for reference Materials and measurements, Belgium, 2pp.

Topley B., and Eyring H. (1934) The separation of the hydrogen isotopes by electrolysis. Part I. *J. Chem. Phys.* **2,** 217–230.

Urey H. C. (1947) The Thermodynamic properties of isotopic substances. *J. Chem. Soc.* **1947,** 562–581.

Walker W. F., Parrington J. R. and Feiner F. (1989) Nuclides and Isotopes. General Electric Company.

Walsh C. (1978) Chemical approaches to the study of enzymes catalizing redox transformations. *Ann. Rev. Biochem.* **47,** 881–931.

Welch S. A., Beard B. L., Johnson C. M., and Braterman P. S. (2003) Kinetic and equilibrium Fe isotope fractionation between aqueous Fe(II) and Fe(III). *Geochim. Cosmochim. Acta* **67,** 4231–4250.

Wiesli R. A., Beard B. L., Taylor L. A., and Johnson C. M. (2003) Space weathering processes on airless bodies: Fe isotope fractionation in the lunar regolith. *Earth Planet. Sci. Lett.* **216,** 457–465.

Young E. D., Galy A., and Nagahara H. (2002) Kinetic and equilibrium mass-dependent isotope fractionation laws in nature and their geochemical and cosmochemical significance. *Geochim. Cosmochim. Acta* **66,** 1095–1104.

Zhang C. L., Horita J., Cole D. R., Zhou J. Z., Lovley D. R., and Phelps T. J. (2001) Temperature-dependent oxygen and carbon isotope fractionations of biogenic siderite. *Geochim. Cosmochim. Acta* **65,** 2257–2271.

Zhu X. K., Guo Y., Williams R. J. P., O'Nions R. K., Matthews A., Belshaw N. S., Canters G. W., de Waal E. C., Weser U., Burgess B. K., and Salvato B. (2002) Mass fractionation processes of transition metal isotopes. *Earth Planet. Sci. Lett.* **200,** 47–62.

Zhu X. K., O'Nions R. K., Guo Y. L., and Reynolds B. C. (2000) Secular variation of iron isotopes in North Atlantic Deep Water. *Science* **287,** 2000–2002.